High strain-rate effects from blast loads on laminated glass: an experimental investigation of the post-fracture bending moment capacity based on time-temperature mapping of interlayer yield stress

S.C. Angelides*[1], J.P. Talbot[1] & M. Overend[2]

[1]Department of Engineering, University of Cambridge, Cambridge, UK

[2]Faculty of Architecture and the Built Environment, Delft University of Technology, Delft, The Netherlands

*** sca36@cam.ac.uk**

Abstract

To enhance the resilience of buildings, laminated glass panels are increasingly used in glazed façades. These ductile panels provide a superior blast resistance to that provided by monolithic glass panels, due to the improved residual capacity offered by the polymer interlayer following the fracture of the glass layers. The complex interaction between the attached glass fragments and the interlayer is still only partially understood. To help address this, this paper investigates experimentally the post-fracture bending moment capacity of laminated glass. Three-point bending tests are performed at low temperature on specimens pre-fractured before testing, to ensure controlled and repeatable fracture patterns. The low temperature simulates the effects of the high strain-rates that result from short-duration blast loads by taking advantage of the time-temperature dependency of the viscoelastic interlayer. In these experiments, polyvinyl butyral is considered as the interlayer, this being the most common interlayer for laminated glass used in building facades. A new time-temperature mapping equation is derived from experimental results available in the literature, to relate the temperatures and strain-rates that result in the same interlayer yield stress. The results of the low-temperature tests demonstrate an enhancement of the ultimate load capacity of the fractured glass by two orders of magnitude, compared to that at room temperature. This suggests an improved post-fracture bending moment capacity associated with the now stiffer interlayer working in tension and the glass fragments working in compression. Due to the time-temperature dependency of the interlayer, a similar enhancement is therefore anticipated at the high strain-rates associated with typical blast loading. Finally, the assumed composite bending action is further supported by the results from additional specimens with thicker PVB and glass layers, which result in enhanced capacity consistent with the bending theory of existing analytical models.

Keywords Laminated glass, Blast response, Strain-rate, Post-fracture, Time-temperature mapping

1 Introduction

Counter-terrorist measures are increasingly being implemented as standard in the design of buildings. It is often recommended that the glazed facades of commercial and residential buildings, which constitute the first barrier of defence in a blast event, include laminated glass panels. These composite glass-polymer sandwich structures are produced by applying heat and pressure to the glass-polymer layers, and provide a superior blast resistance to that provided by monolithic glass panels. This is due to the improved residual capacity offered by laminated glass, which, unlike brittle monolithic glass, provides resistance to the blast wave after the glass layers have fractured. In addition, after fracture, most of the glass fragments are held together by the polymer interlayer, thereby reducing the risk of glass-related injuries.

The interlayers are manufactured from either polymer films or liquid resins. The most common interlayer used in laminated glass for building facades is polyvinyl butyral (PVB). This thermoplastic polymer was first developed for the automotive industry in the 1950s, with the construction industry adopting its use in the 1970s [1]. Its key attributes are its ability to block UV radiation, its high strain to failure and its good adhesion properties, which enable it to retain the glass fragments after fracture. PVB is the preferred interlayer recommended by the Centre for the Protection of National Infrastructure (CPNI) for blast-resistant glazing applications. Commonly encountered, commercially available PVB products include Butacite® and Trofisol® (from Kuraray), Saflex®

(from Eastman), Lam 51H® (from Everlam) and S-Lec™ (Sekisui) [2]. More recently, ionomer interlayers, such as Kuraray's SentryGlas® (previously manufactured by DuPont) have been developed with the aim of improving the stiffness and tensile strength of PVB. Although ionomer interlayers are also permitted by CPNI [2] for enhancing the blast protection of buildings, more typical applications are to provide stiffer panels for large spans and to improve impact resistance. Thermoplastic polyurethane (TPU), ethyl vinyl acetate (EVA) and poured resin (liquid resin cast in-situ) are alternative, commercially available interlayers, although they are not recommended by CPNI [2] for blast applications. The focus of this paper is therefore laminated glass with PVB interlayer.

The blast response of PVB-laminated glass panels, and particularly the post-fracture response, when all glass layers have fractured, is a complex multi-disciplinary problem that is still not well understood. Full-scale blast tests have been performed by various researchers to study this, using high-explosive detonations [3–8] and shock-tube simulations [3,9–11]. These tests typically focus on recording the global peak-displacement time-history of the panel through all stages of deformation. The failure mechanisms of these panels can also be observed from these full-scale blast tests. This usually involves a ductile response, with the PVB tearing either from large strain accumulation or cutting from the attached glass fragments [9]. Pelfrene et al. [10] commented, however, that a brittle failure occurs for panels with a high adhesion level between the PVB and the glass layers. This is attributed to the restriction of local delamination that results in the rapid accumulation of strains and subsequent premature tearing of the PVB. The adhesion level, which varies for different products, is therefore an important parameter for the blast response. Hooper [5] reports of a consistent, doubly-symmetric fracture pattern forming, resembling a central rectangle connected by four diagonals to the corners of the panel. This pattern is formed from small glass fragments that, in some cases, are crushed by the large strains in these regions. Within the rectangle, the fragments are large and irregular in shape, ranging from 30 mm to 40 mm in size, while between the rectangle and the panel edges the fragments are smaller, with measurements indicating fragments as small as 3 mm in size.

Important information can be inferred from this observed pattern, when compared to the equivalent response of monolithic glazing. The blast failure of monolithic annealed glazing results in multiple glass fragments that are described as sharp, angular and irregular in shape and size [12]. This is a consequence of rapid crack propagation that is initiated when tensile stresses, caused by the combined out-of-plane bending and membrane response of the intact panel, exceed the fracture stress of glass (i.e. the stress at which cracking begins). It may therefore be inferred that the fracture pattern observed in laminated glass is the result of two stages: an initial global fracture pattern, similar to the response of monolithic glazing, followed by additional local fracture. The latter is attributed to the crushing of glass fragments from large compressive strains that are caused by the out-of-plane bending of the fractured panel. The consistent pattern formed from small glass fragments that was observed by Hooper [5], therefore represents a yield line mechanism. As described in the analytical models developed by Angelides et al. [13], the formation of plastic hinges may be attributed to a composite bending action, with the interlayer acting in tension and the compression component being provided by the glass fragments that come into contact as the panel deforms. For large deflections, the result is a combined bending and membrane response. This hypothesis has not been experimentally validated, as full-scale blast tests provide no information on the relative contribution of bending moments and membrane forces to the post-fracture capacity of a panel. The need for small-scale, complementary experiments is therefore evident, to understand the fundamental underlying mechanics of the panel post-fracture blast response that is obscured in full-scale tests.

This need has been recognised by many researchers, who have performed such experiments to investigate the post-fracture membrane capacity of laminated glass. Due to the viscoelastic nature of PVB, which is time dependent, these typically involve high-speed tensile tests on PVB alone to investigate experimentally the effects of the high strain-rates that result from short-duration blast loads [4,14–21]. Hooper [5] and Samieian et al. [22] performed similar tests but on pre-fractured laminated glass specimens. These experiments highlighted the importance of the delamination of glass fragments that allow a ductile response to occur, as opposed to the brittle failure previously discussed for panels with high adhesion. It was also shown that the attached glass fragments have a stiffening effect on the PVB. To model the anticipated fracture pattern of laminated glass from blast loads, Hooper [5] considered three uniform, pre-fractured patterns; two regular patterns (based on 10 mm and 20 mm glass fragments) and one random pattern.

Unlike the post-fracture membrane response, to the authors' knowledge, the post-fracture bending moment capacity of laminated glass at high strain-rates has not been previously investigated experimentally with small-scale bending experiments. The bending response at low strain-rates has been the focus of many researchers, such as Kott and Vogel [14,23,24] and Botz [25]. The former performed four-point bending tests on simply-supported, axially unrestrained, specimens and concluded that the residual capacity of fractured, laminated glass is negligible compared to the intact capacity. However, this conclusion overlooks the fact that the response is fundamentally different under short-duration blast loading due to the viscoelastic nature of PVB. Botz [25] assessed the creep

response of pre-fractured specimens loaded in bending. Once again, these experiments showed the importance of local delamination of glass fragments to prevent a brittle failure.

This paper aims to contribute to our understanding of the blast response of laminated glass by focussing on its post-fracture bending capacity at high strain-rates. Although membrane action is anticipated to dominate the response at large deflections, as demonstrated by the yield condition defined by Angelides et al. [13], the investigation of the residual bending capacity is important, as it is expected that strains will accumulate along the yield lines formed during bending, dissipating energy and ultimately leading to tearing failure of the PVB. Two objectives are set for the experimental work presented here. Firstly, to demonstrate that the bending capacity is significantly enhanced at high strain-rates due to stiffening of the PVB. To achieve this, the ultimate load capacity of fractured laminated glass in pure bending will be compared at low and high strain-rates. The second objective is to investigate if the post-fracture response of laminated glass can be described using cracked elastic theory, which assumes a composite bending action of the interlayer, working in tension, together with the glass fragments working in compression. In particular, the experimental results will assist in validating the analytical models developed by Angelides et al. [13], which predict the elastic bending capacity at high strain-rates using an equivalent, transformed cross-section. This elastic response was identified as Stage 3 by Angelides et al. [13], with Stage 4 corresponding to the subsequent plastic response. Note that the terms ‘elastic’ and ‘plastic’ used here refer to the change in stiffness observed in the post-fracture stress-strain diagram.

Traditional dynamic bending tests result in both inertia and strain-rate effects. This complicates the experimental derivation of the bending capacity because dynamic amplification effects contribute to the response, in addition to the enhanced material properties at the high strain-rates. This work focusses on the latter as an intermediate step to validating experimentally our understanding of the composite bending action of the attached glass fragments and the now stiffer PVB (future work using dynamic bending tests will study the inertia effects). An alternative, small-scale experimental procedure is presented that decouples the inertia loading from the effects of high strain-rate. This is achieved by performing low strain-rate, quasi-static, bending tests at low temperature to simulate the effects of high strain-rate. Although typical strain-rates associated with blast loading are considered here, the conclusions from this paper can also be applied to other load cases that result in high strain-rates, such as impact loading.

The time-temperature dependency of polymers is central to the experimental approach. The paper therefore begins with a discussion of its application to PVB, including a new time-temperature mapping for the PVB yield stress that is derived from experimental results available in the literature. The experimental work performed on pre-fractured laminated glass is then described, followed by the results and a discussion of the influence of low temperature. Finally, the results are compared with the analytical predictions of Angelides et al. [13].

2 Time-temperature mapping for PVB yield stress

The material properties of viscoelastic polymers depend on both time and temperature. In this section, the temperature and strain-rate dependency of PVB is first discussed, followed by the derivation of a linear time-temperature mapping equation. This forms the basis for the experimental work described in Sections 3 and 4, which aims to simulate the effects of high strain-rate with low temperatures.

2.1 Temperature dependence

PVB is an amorphous thermoplastic polymer [26]. It therefore has a glass transition temperature (T_g), which corresponds to a phase transition between a rubbery and a glassy state. The glass transition temperature for an amorphous polymer can be derived experimentally using a relaxation method, such as a Dynamic-Mechanical-Thermal Analysis (DMTA), which is performed by imposing a cyclic stress on a specimen and measuring the corresponding strain response [27]. Such analyses have been performed by Hooper [5], Liu et al. [28], Kuntsche [29], Pelayo et al. [30] and Kraus [31] to characterise the viscoelastic response of PVB over a range of temperatures. Alternative thermal analysis methods to determine the glass transition temperature include Thermomechanical Analysis (TMA) and Differential Scanning Calorimetry (DSC) [31]. For Saflex® PVB, Hooper [5] concluded that the state is glassy below 5 ˚C, and rubbery above 40 ˚C. Between these two temperature limits the response is in a transition phase. It should be noted that the value of the glass transition temperature for PVB depends on the percentage and type of plasticizer used, and therefore varies between manufacturers [26,31]. Hooper [5] concluded that Butacite® PVB has a glass transition temperature between 5 ˚C and 10 ˚C higher than Saflex®, while Kraus [31] observed the transition phase for Trofisol® (BG R20) to occur between 20 ˚C and 30 ˚C.

2.2 Strain-rate dependence

In addition to temperature, polymers are also sensitive to strain-rate. Walley et al. [32] performed multiple, high strain-rate tests on various polymers, and categorised them into three groups based on the observed relationship between yield stress and the logarithm ($\log_{10}$) of strain-rate. When expressed in this way, a bi-linear relationship, with a sharp increase in gradient at high strain-rates, was observed consistently for one of the three polymer groups identified. It was concluded that this bi-linearity is due to lower order relaxation processes of the polymers, which are known to occur at low temperatures, also occurring at room temperature under sufficiently high strain-rates [33]. For polymers exhibiting this bi-linear relationship, the yield stress is therefore time-temperature dependent. This raises the question as to whether or not similar behaviour is observed in PVB.

To answer this question, we consider the experimental results of Chen et al. [20], who performed tensile tests on Butacite® PVB at strain-rates ranging from 0.1 s^{-1} to 300 s^{-1} at four different temperatures: -30 ˚C, -5 ˚C, 25 ˚C and 40 ˚C. Figure 1 replots the yield stress values recorded by Chen et al. [20] but now plotted against the logarithm ($\log_{10}$) of strain-rate and using the mean value of the yield stress results obtained at each strain rate (actuator speed). It should be noted that the yield stress here refers to the stress at which a significant change in modulus is observed which is manifested in a change in slope of the stress-strain diagram, rather than the onset of true plasticity [13]. A linear relationship is clearly evident in Figures 1a and 1b for temperatures between -30 ˚C and -5 ˚C, which is consistent with the PVB being below its glass transition temperature and therefore in a glassy state for all strain-rates. A small deviation from this linear relationship is evident at some points – notably Points A, B and C in Figure 1a – but this is most likely attributable to the experimental challenges of recording with precision the yield stress of PVB at low temperatures. At the higher temperatures of 25 ˚C and 40 ˚C (Figures 1c and 1d), the relationship is distinctly bilinear, exhibiting a transition from a shallow to a steeper slope at high strain-rates, and corresponds to a transition from rubbery to glassy state. The graph of Figure 1c also shows remarkable agreement with the results of Hooper's [5] DMTA tests, which concluded that the glass transition temperature increases from 5 °C to 20 °C at a strain-rate of 3.2 s^{-1} ($\log_{10}[3.2\,] = 0.51$). It should be noted that Hooper [5] performed tests on Saflex® PVB at 20 °C, whereas the plot in Figure 1c is for Butacite® PVB at 25 °C. Nevertheless, these observations provide strong evidence for a glass transition of PVB occurring at room temperature as a direct result of high strain-rate.

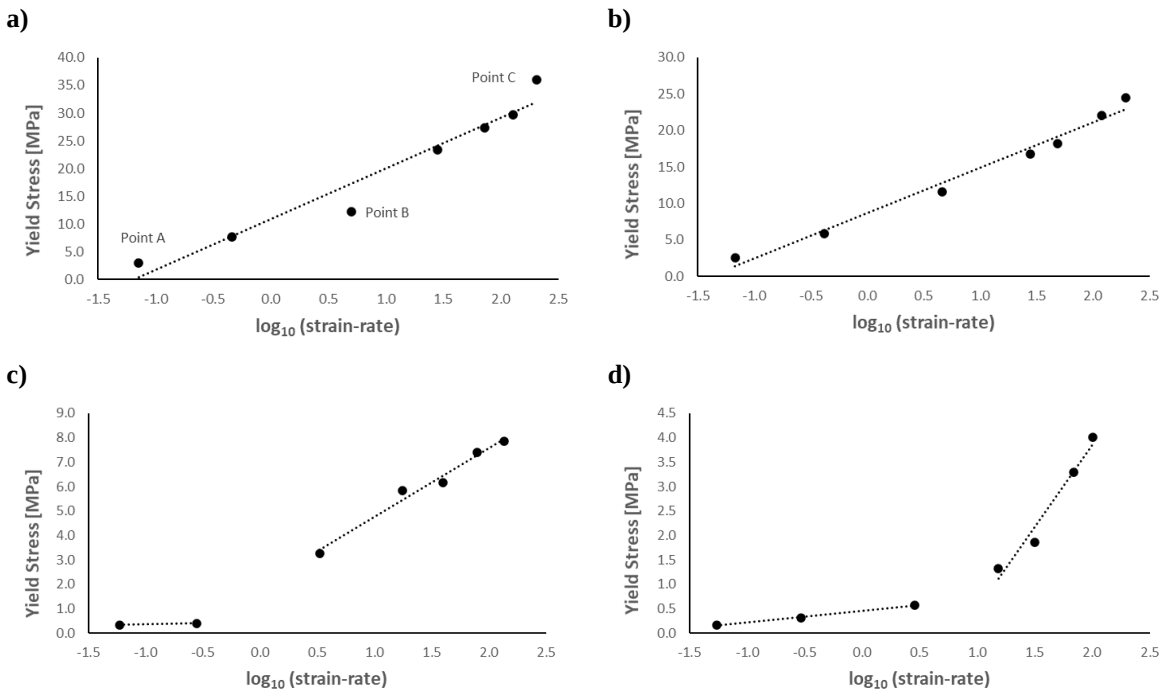

Fig. 1 Plots of yield stress vs logarithm ($\log_{10}$) of strain-rate, derived from experimental results presented by Chen et al. [20] at different temperatures: (a**)** -30 ˚C, (b) -5 ˚C, (c) 25 ˚C and (d) 40 ˚C.

Under short-duration blast loading, it is therefore expected that the response of PVB will be fundamentally different to long-duration static loading. Morison [4] presented results from full-scale blast tests performed at 20 ˚C and reported mean strain-rates ranging from 7.6 s^{-1} to 17.5 s^{-1} in fractured, laminated glass panels. These strain-rates are clearly high enough for the PVB to be in the (stiffer) glassy state, which results in enhanced yield

stress values, thereby providing a higher post-fracture bending moment capacity of the laminated glass than would be possible in the rubbery state.

2.3 Linear time-temperature equivalence mapping for PVB yield stress

It is evident that the PVB yield stress is sensitive to both strain-rate and temperature, with a potential time-temperature dependency similar to many other polymers. Williams et al. [34] developed an empirical equation – the Williams-Landel-Ferry (WLF) equation – to model the time-temperature equivalence of amorphous polymers. Hooper [5], Liu et al. [28], Kuntsche [29], Pelayo et al. [30] and Kraus [31] showed this to be applicable to PVB. However, the WLF equation is recommended only for temperatures above the glass transition temperature. Siviour et al. [35] developed an alternative equation to map the dependence of yield stress to strain-rate and temperature for polycarbonate (PC) and polyvinylidene difluoride (PVDF). This approach requires the determination of a single empirical parameter and Siviour et al. [35] demonstrated good agreement with experimental results spanning over phase transitions (i.e. different states). The resulting mapping equation was later applied to many other polymers, also proving to provide good agreement with experimental results [33,36–39]. The application of this approach to temperatures below the glass transition temperature has provided the motivation for the work reported here, which seeks to use low temperatures as a proxy for the high strain-rates experienced by PVB during blast loading.

The yield stress values for PVB recorded by Chen et al. [20] at 25 ˚C may be compared with those recorded at -30 ˚C, -5 ˚C and 40 ˚C but now mapped to 25 ˚C using the linear time-temperature equivalence mapping equation derived by Siviour et al. [35]:

$$T_{map} = T_{exp} + \lambda\left(\log_{10}\dot{\varepsilon}_{map} - \log_{10}\dot{\varepsilon}_{exp}\right) \tag{1}$$

where T_{exp} and $\dot{\varepsilon}_{exp}$ are the temperature and strain-rate corresponding to a measured yield stress data point, while T_{map} is the mapped temperature, of the same yield stress, corresponding to a strain-rate of $\dot{\varepsilon}_{map}$. The constant λ is determined by considering two data points with the same yield stress ($\sigma_{\mathrm{y,i}} = \sigma_{\mathrm{y,ii}}$) measured at different temperatures (T_i, T_{ii}) and strain-rates ($\dot{\varepsilon}_i, \dot{\varepsilon}_{ii}$):

$$\sigma_{y,i}(T_i,\ \dot{\varepsilon}_i) = \sigma_{y,ii}(T_{ii},\ \dot{\varepsilon}_{ii}) \ \Rightarrow \quad \lambda = \frac{T_{ii} - T_i}{\log(\dot{\varepsilon}_{ii}) - \log(\dot{\varepsilon}_i)} \tag{2}$$

From Chen et al.'s [20] data, re-plotted in Figure 1, it is possible to identify two different states that correspond to a similar yield stress. These are summarised in Table 1. Using these values, Equation 2 yields a mapping constant of $\lambda = 18.44$. Substituting this into Equation 1 allows us to map (i.e. convert) the yield stress values originally measured at -30 ˚C, -5 ˚C and 40 ˚C to the yield stress values expected at 25 ˚C (Figure 2). This figure excludes strain-rate data below 3.2 s^{-1} ($\log_{10}[3.2\,] = 0.51$), because PVB is in a non-glassy state that is of no interest for blast response. The results are promising, showing good agreement with the measurements at 25 ˚C, and clearly indicate a linear relationship for these mapped values. Some deviation from this relationship is observed in a few mapped points, with the largest discrepancy noted for Points A, B and C (see Figure 2). However, these three points correspond to the measurements at -30 ˚C that are highlighted with the same labels in Figure 1a and whose accuracy was questioned in Section 2.2.

To gain further confidence in the proposed time-temperature mapping, Figure 2 includes the yield stress values measured independently during high-speed tensile tests at room temperature by Bennison et al. [15], Iwasaki et al. [16], Hooper [5] and Zhang et al. [19]. The values from Zhang et al. [19] are mean values obtained from tests performed multiple times at the same strain rate (actuator speed) on nominally identical specimens. It should also be noted that the tests of Bennison et al. [15], Iwasaki et al. [16] and Hooper [5] were performed at ambient laboratory temperature but the exact temperature is unknown, whereas Zhang et al. [19] performed their tests at 30 ˚C and not the mapping temperature of 25 ˚C. Furthermore, Hooper's [5] tests were performed on Saflex®, whereas our mapping is based on the work of Chen et al. [20] that was performed on Butacite® (Iwasaki et al. [16] and Zhang et al. [19] do not record the manufacturer of their PVB). Given these differences and uncertainties, the results are all in good agreement with the proposed time-temperature mapping, and it is therefore concluded that this offers an effective means of simulating the effects of high strain-rate on PVB.

State	Temperature [˚C]	Strain-rate [s^{-1}]	Yield Stress [MPa]
i	-5	0.41	5.85
ii	25	17.48	5.82

Table 1 Two different PVB states (temperature, strain-rate) with similar yield stress values, based on the mean experimental results of Chen et al. [20].

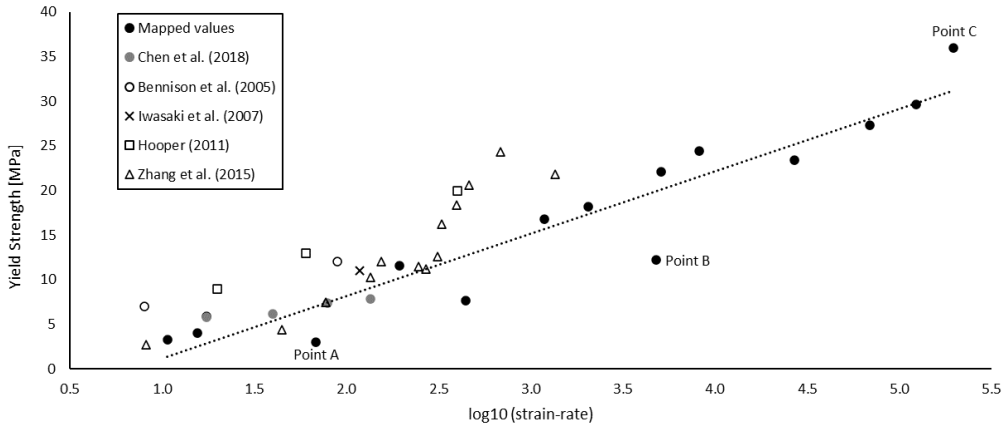

Fig. 2 Variation of yield stress with strain-rate, comparing the mapped values at 25 ˚C (from experimental measurements of Chen et al. [20] at -30 ˚C, -5 ˚C and 40 ˚C) with experimental values from Bennison et al. [15], Iwasaki et al. [16], Hooper [5], Zhang et al. [19] and Chen et al. [20] at room temperature.

3 Experimental method

This section describes the experimental method. The testing facilities and the glass specimens are first introduced, followed by a description of the bending tests performed at low temperature to demonstrate the enhanced ultimate load capacity at high strain-rates. The validation of existing analytical solutions using the experimental results is then explained.

3.1 Experimental facilities and laminated glass specimens

The experiments were performed in Cambridge University Engineering Department using a Schenck Hydropuls PSA testing machine within an environmental chamber. The PSA machine is typically used for axial testing, but bending tests can also be performed by incorporating a three-point bending test (3-PBT) rig, as shown in Figure 3. The span *L'* between the simple-supports is 110 mm, with the load applied mid-span. The maximum load cell capacity is 10 kN, and the displacement is measured from the movement of the loading piston. Temperatures as low as -196 ˚C can be achieved in the chamber using a thermostatically regulated supply of liquid nitrogen.

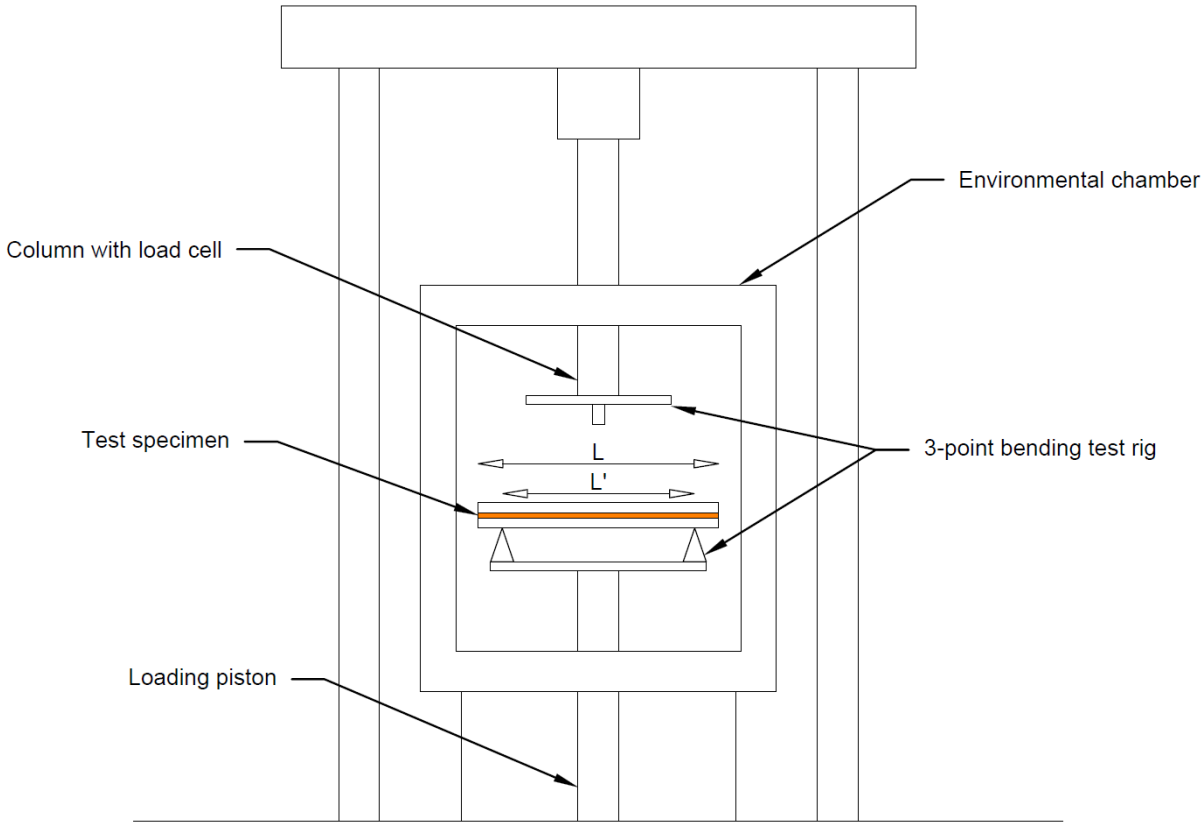

Fig. 3 Schematic diagram of the low-temperature test rig, illustrating the three-point bending test of a laminated glass specimen.

The test specimens consisted of laminated glass made from two layers of annealed glass, with polished edges (to minimise secondary cracking) and a PVB interlayer. The overall geometry of the specimens (total length L = 200 mm and width B = 55 mm) was determined by the available space within the chamber and the need to ensure a sufficiently high length-to-thickness ratio for bending; the thickness of each layer was dictated by manufacturing constraints. Three different cross-sections were tested in total, with the same length and width but different thicknesses of glass and PVB, as summarised in Table 2. The specimens were laminated in a commercial, glass laminating autoclave by Phoenicia (CS1) and ToughGlaze (CS2, CS3) to BS EN ISO 12543-2[40].

*The ambient temperature varied between approximately 25 and 28 ˚ C.

CROSS-SECTION	NUMBER OF SPECIMENS	TEMPERATURE [˚C]	LENGTH (L) [mm]	WIDTH (B) [mm]	GLASS THICKNESS (t_G) [mm]	PVB THICKNESS (t_{PVB}) [mm]
CS1	3	~25*	200	55	3	0.38
	3	-100				
CS2	3	-100	200	55	3	1.52
CS3	3	-100	200	55	6	1.52

Table 2 Geometrical properties and testing conditions of laminated glass specimens.

To ensure controlled and repeatable fracture patterns, the specimens were pre-fractured before testing, by first scoring both glass faces with a glass cutter and then impacting them at the location of the score, from both sides, to produce full-thickness cracks in each glass layer. Similar methods of pre-fracturing have been described by Nhamoinesu & Overend [41], Hooper [5] and Samieian et al. [22]. Although a random pattern of irregular fragments occurs under blast loading, the pattern considered here is idealised as a series of cracks at a uniform distance of 20 mm crack spacing to allow direct comparison between tests and elicit the fundamental behaviour. Each specimen was pre-fractured immediately before testing, to avoid the need for controlled storage of pre-

fractured specimens. This minimised the influence of any moisture on the exposed PVB, which could have led to degradation in material properties [25,42].

3.2 Instrumentation and temperature control

The bending tests were carried out at a controlled temperature of -100 ˚C, repeating each test three times to obtain confidence in the experimental results. Displacement-controlled tests were performed at a rate of 0.1 mm/min, with the applied load measured by the 10 kN load cell. The displacement rate was chosen through trial and error; initial tests at a rate of 1 mm/min resulted in instantaneous failure, while secondary tests at a slower rate of 0.01 mm/min proved impractical due to the time and volume of liquid nitrogen required. The combined experimental temperature ($T_{exp} = -100$ ˚C) and displacement-rate (which results in a strain-rate $\dot{\varepsilon}_{exp}$) were chosen using Equation 1 to simulate the effect of high strain-rate ($\dot{\varepsilon}_{map}$) associated with blast loading at room temperature ($T_{map} = 25$ ˚C). Lower or higher experimental temperatures could also be considered to examine the post-fracture bending moment capacity of laminated glass at temperatures below or above the room temperature, respectively. The temperature in the environmental chamber was controlled through an internal thermometer and verified with a thermocouple placed near the specimens. To ensure that the specimens themselves reached the desired temperature, a second thermocouple was initially bonded to a sample specimen to establish the time required for its temperature to reach that of the chamber. This time was found to be approximately 10 minutes and this acclimatisation period was used in all specimens prior to testing. To verify that the PVB itself was also cooled to the desired temperature, a thermal camera was used (see Figure 4). Although this indicates a temperature of -39.9 ˚C (as there is a loss of cooling as soon as the chamber is opened to record the image) it is clear that the temperatures of the glass and PVB layers are within a few degrees of each other. To assess the influence of high strain-rates, the CS1 pre-fractured specimens were also tested at room-temperature using the same test rig, at the same displacement-rate, but without the liquid nitrogen cooling. Again, each test was repeated three times. The ultimate loads measured at both low and room temperature were then compared.

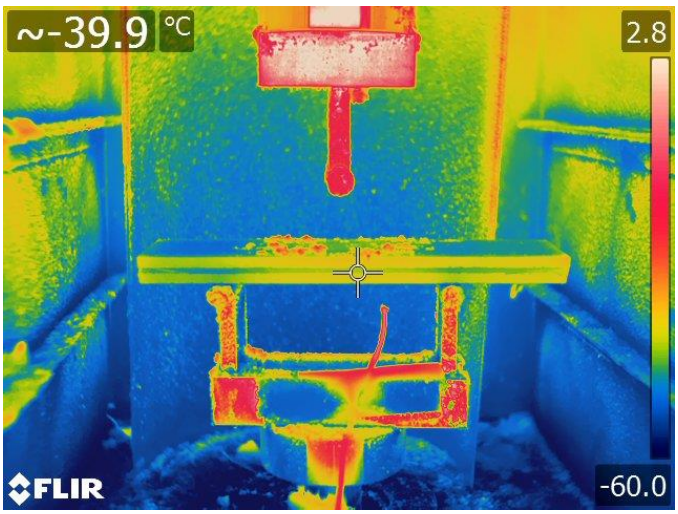

Fig. 4 Thermo-graphic image used to assess the uniformity of temperature between the glass and PVB.

3.3 Validation of analytical models

A key objective of the experimental work is to help validate the analytical models of Angelides et al. [13], which predict the post-fracture bending capacity of laminated glass in the absence of inertia effects. The post-fracture moment capacity can be derived from the experimental results by considering the associated bending moment diagram. For the three-point bending tests performed, this indicates a maximum elastic moment of:

$$M_{max} = \frac{PL'}{4} \tag{3}$$

For these simply-supported, statically determinate specimens, the bending moment distribution is governed by equilibrium alone and is not affected by the stiffness variation along the span resulting from the pre-fractured cracks. The experimentally derived, elastic capacity ($M_{3,E}$) corresponds to the maximum load of the linear response observed in the load *vs* mid-span displacement diagram:

$$M_{3,E} = \frac{P_3 L'}{4} \tag{4}$$

where P_3 is the elastic load capacity. The experimentally derived, plastic capacity ($M_{4,E}$) corresponds to the ultimate load:

$$M_{4,E} = \frac{P_4 L'}{4} \tag{5}$$

where P_4 is the ultimate load capacity. It should be noted that the linear response assumed only holds for the simply-supported specimens tested here, as the response becomes nonlinear for axially restrained specimens, due to the development of membrane forces under large deflections (nonlinear equilibrium relationship) and the presence of large rotations (nonlinear compatibility relationship).

These experimental moment capacities are compared with the analytical expressions derived by Angelides et al. [13]. The elastic bending capacity ($M_{3,A}$ corresponding to Stage 3) was derived using an equivalent, transformed cross-section, while the plastic capacity ($M_{4,A}$ corresponding to Stage 4) was derived by applying moment equilibrium about the plastic neutral axis (Stages 1 and 2 correspond to the pre-fracture response). These analytical expressions are reproduced as Equations A1 and A2 in Appendix A. In the calculation of the analytical moment capacities, the yield strength of PVB is based on the results of Hooper's [5] high-speed tensile tests on pre-fractured specimens, as described in Section 1. The yield strength depends on three parameters: glass fragment size, PVB thickness and strain-rate. The latter requires a mapping, using Equation 1, from the current experimental strain-rate at -100 ˚C to the equivalent rate of Hooper's [5] room-temperature tests. The maximum experimental strain-rate is derived based on the assumption of plane sections remaining plane:

$$\dot{\varepsilon} = \dot{\kappa} y_{3,PVB} \tag{6}$$

where $\dot{\varepsilon}$ is the strain-rate, $\dot{\kappa}$ is the curvature rate and $y_{3,PVB}$ is the distance of the extreme PVB fibre from the elastic neutral axis. Considering the linear-elastic response up until the point of yield, the curvature rate can be expressed in terms of the moment rate:

$$\dot{M} = \frac{\dot{P} L'}{4} = EI\dot{\kappa} \tag{7}$$

where $\dot{P}$ is the loading rate, which can be calculated from the slope of the load time-history. Finally, the bending stiffness (EI) is obtained by comparing the slope of the recorded load (P) vs mid-span displacement ($\delta_{v,mid}$) diagram with its theoretical value:

$$\delta_{v,mid} = \frac{P L'^3}{48EI} \tag{8}$$

It should be noted that the low-temperature experimental method does not capture the effects of high strain-rate on the glass layers, which are known to exhibit both enhanced tensile fracture strength and compressive crushing strength [13]. The latter influences the plastic capacity, as this dictates the location of the plastic neutral axis. The experimental results should therefore result in a lower, plastic capacity compared to the analytical model, which assumed an enhanced compression strength of glass derived from Split Hopkinson Pressure Bar tests. Additionally, the presence of frost during the low temperature tests may also reduce the PVB modulus at crack locations, due to elevated moisture levels. Such degradation was observed by Botz et al. [42] and Botz [25], although their specimens were conditioned for at least 24 hours under increased moisture, whereas the specimens tested here at low temperature were exposed to increased moisture for less than 1 hour (see Section 4.1). Nevertheless, this would result in a conservative estimation of the moment capacities at high strain-rates. Finally, the low temperature results in a stiffer adhesion bond that inhibits the delamination of the glass fragments and causes brittle failure of the PVB, as reported by Samieian et al. [22] following high strain-rate tensile tests on pre-fractured specimens at various temperatures. This, however, does not affect the experimental work presented here, as the scope is limited to validating the post-fracture bending moment capacities, and does not include the response beyond the formation of a plastic hinge.

4 Results and Discussion

This section presents the results of the experimental work described in Section 3. Firstly, a comparison of the ultimate loads recorded at low and room temperature is presented for the CS1 specimens. These results, together with those from the thicker CS2 and CS3 specimens, are then compared with the analytical solutions from Equations A1 and A2.

4.1 Comparison of ultimate load at room and low temperatures

Figures 5 and 6 provide an overview of the tests. At low temperature, these concluded with the PVB tearing in a brittle manner at the mid-span crack, as shown in Figure 5c. The local delamination evident in the vicinity of the glass cracks in Figure 5c is a result of the pre-fracturing process and not of the bending tests. At room temperature, the response is more ductile, with the specimens able to deform to large deflections without tearing the PVB, as shown in Figure 6. In this case, the tests were terminated when the applied load reached a plateau. The average test duration was 41 minutes at low temperature and 153 minutes at room temperature.

a) **b)**

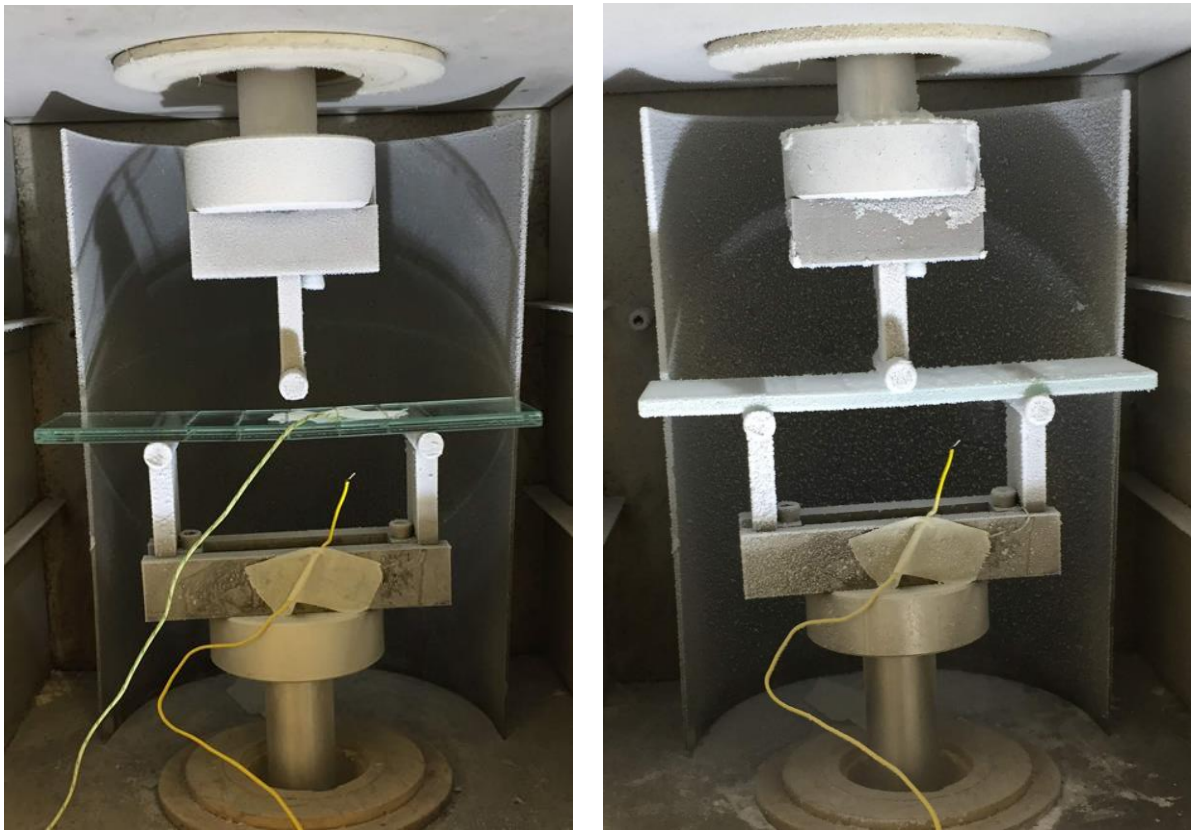

c)

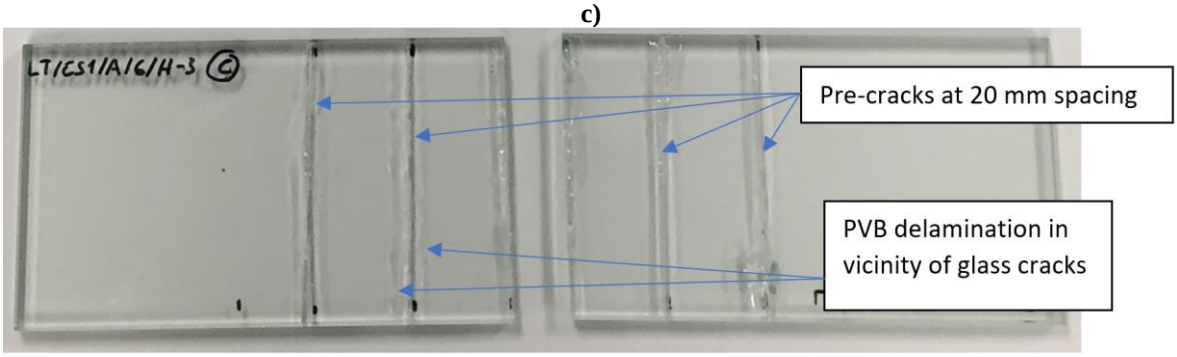

Fig. 5 Quasi-static, three-point bending test of pre-fractured laminated glass, with uniform pattern, at low temperature: (a**)** cooling of environmental chamber, (b) testing at -100 ˚C, (c) brittle failure from PVB tearing at the mid-span crack.

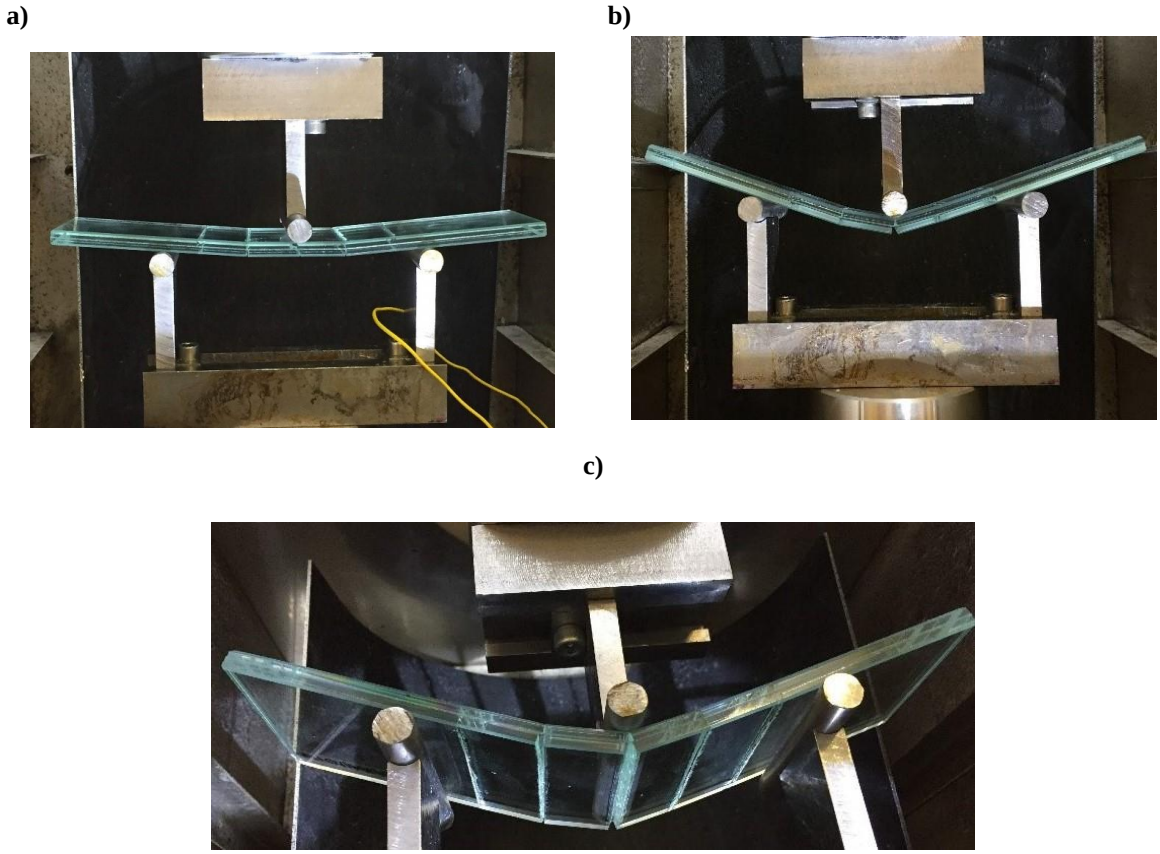

Fig. 6 Deformation of pre-fractured laminated glass, with uniform pattern, during quasi-static testing at room temperature: (a) small deflections, (b) large deflections, (c) close-up view.

The ultimate load measurements from the testing of the CS1 specimens are summarised in Table 3. It was challenging to produce identical fracture patterns and to maintain a constant temperature throughout the duration of the tests. In addition, there is inherent variability in the material properties. Nevertheless, the low-temperature results show a relatively good consistency across the three, nominally identical, tests. The results at room temperature vary more significantly in relative terms. The accuracy of these was primarily limited by the sensitivity of the available load cell, which had a capacity 10 kN, far in excess of the ultimate loads measured (1-4 N), as it was decided to use the same experimental facilities for both low and room temperature tests. Nevertheless, these results are considered sufficient for the assessment of the low temperature effects (and therefore high strain-rate effects), which is the primary objective of this paper. A further limitation may have been the inability to control the room temperature precisely. However, these limitations do not detract from the primary observation: that the ultimate load at low temperature is two orders of magnitude higher than that at room temperature.

TEMPERATURE	ULTIMATE LOAD [N]			
	TEST 1	TEST 2	TEST 3	AVERAGE
Room (~25 ˚C)	3.82	1.33	1.69	2.28
Low (-100 ˚C)	269.70	196.43	242.69	236.27

Table 3 Recorded ultimate load from the low- and room-temperature tests of the CS1 specimens with a uniform pre-fractured pattern.

This significant difference in ultimate load is evident in Figure 7, which shows the recorded load vs mid-span displacement response from all three specimens tested at both temperatures. A stiffer response, resembling a bi-

linear, elastic-plastic load-deflection curve with a brittle failure is observed for the low-temperature tests, where the PVB is in a glassy state (i.e. below its glass transition temperature). In contrast, at room temperature, the PVB is in a transition state and this manifests itself as a more flexible and viscoelastic response.

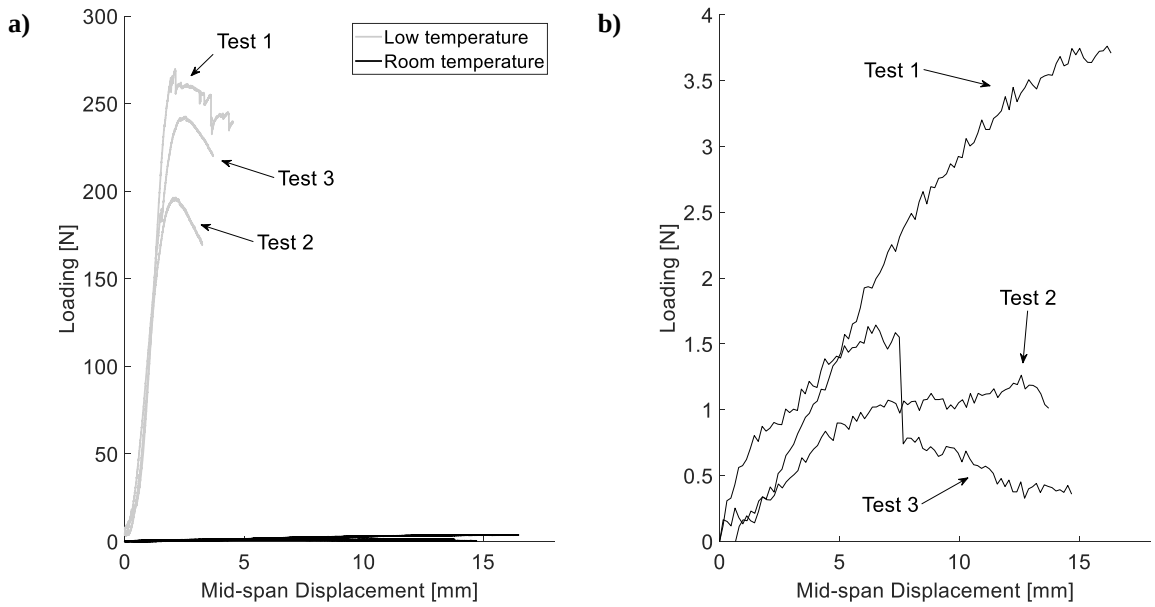

Fig. 7 Load-displacement diagrams from the 3-PBT of the CS1 specimens with a uniform fracture pattern, showing (a) all results and (b) the room-temperature results on a reduced scale.

4.2. Comparison with analytical models

The low-temperature, load-displacement curves of Figure 7a are reproduced separately in Figure 8 for comparison with the analytical models. Four distinct stages of deformation can be identified, and these are labelled in Figure 8 (Stages a-d). Stage a is limited to small loads and corresponds to a flexible response of the PVB. It is believed that this initial stage occurs prior to the glass fragments interlocking.

Stage b is described by a stiffer, linear response, as indicated by the dashed lines, and this corresponds to Stage 3 of the analytical models. At this stage, the PVB stills behaves elastically, as illustrated in Figure 9a. The point at which the post-fracture elastic moment capacity ($M_{3,E}$) is reached for each test is labelled in Figure 8 and summarised in Table 4, together with the derived maximum strain-rate for each test mapped to 25 ˚C. At this strain-rate, of approximately 25 s^{-1}, the yield strength of the PVB is expected to lie in the region of 62 MPa, which is the peak value obtained by Hooper [5] from tensile tests on similar specimens (0.38 mm PVB thickness and 20 mm uniform fracture pattern) at a strain-rate of 30 s^{-1}. It should be noted that Hooper [5] commented that the accuracy of his recorded peak stresses diminished for strain-rates beyond 10 s^{-1} due to experimental limitations. Additionally, the mapping used here, as presented in Section 2, was performed for Butacite® PVB, whereas Hooper's [5] specimens used Saflex®. For a yield strength of 62 MPa, Equation A1 predicts a moment capacity of $M_{3,A} = 3.52$ Nm. This is slightly below the average experimental value of $M_{3,E} = 4.92$ Nm but is nevertheless in reasonable agreement given the uncertainty associated with the yield strength. It is expected that at temperatures below or above the room temperature, this moment capacity would increase or decrease, respectively, due the PVB temperature dependency described in Section 2.1.

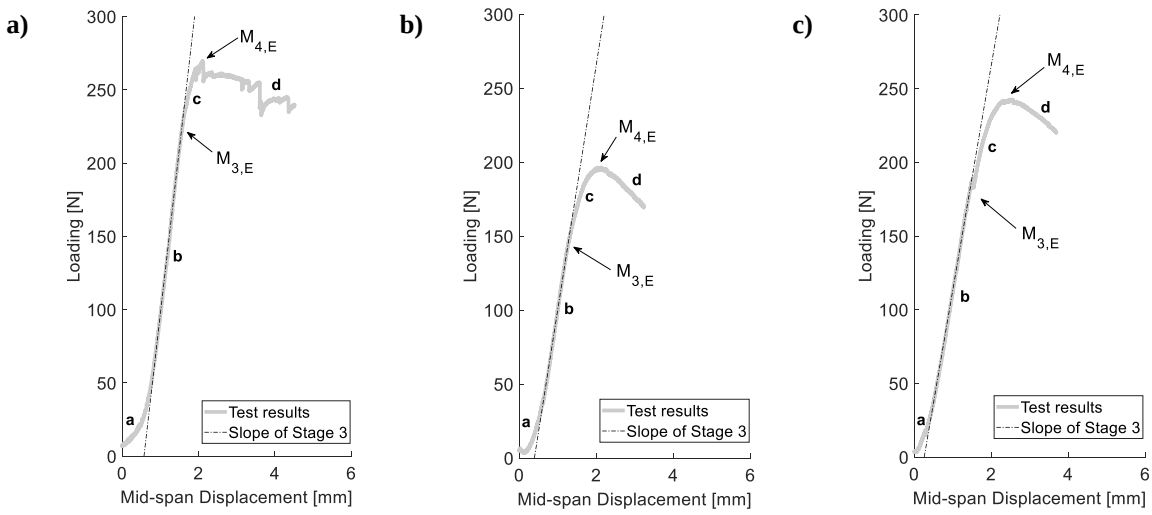

Fig. 8 Individual load-displacement diagrams from the low-temperature tests, reproduced from Fig. 7 to indicate the points at which the elastic ($M_{3,E}$) and plastic ($M_{4,E}$) moment capacities are achieved: (a) Test 1, (b) Test 2 and (c) Test 3.

	TEST 1	TEST 2	TEST 3	AVERAGE
Elastic moment capacity, $M_{3,E}$ [Nm]	5.96	3.89	4.91	4.92
Plastic moment capacity, $M_{4,E}$ [Nm]	7.42	5.40	6.67	6.50
Mapped strain-rate at 25 ˚C [s^{-1}]	25.26	25.29	25.23	25.26

Table 4 Post-fracture elastic ($M_{3,E}$) and plastic ($M_{4,E}$) moment capacities derived from the low-temperature tests, together with the mapped strain-rate at 25˚C: 3-PBT of CS1 specimens with uniform fracture pattern.

Stage c corresponds to Stage 4 of the analytical models. At this nonlinear stage, it is considered that the PVB has yielded and the plastic moment capacity ($M_{4,E}$) is achieved when the glass crushes. The idealised collapse mechanism following the plastic hinge formation is shown in Figure 9b. As mentioned in Section 3.3, the plastic moment capacity is expected to be higher under blast loading due to the enhanced crushing strength of the glass at high strain-rates, which was not captured in the experiments. Nevertheless, Equation A2 predicts a moment capacity of $M_{4,A} = 4.10$ Nm, which is less than the average experimental value of $M_{4,E} = 6.50$ Nm. Again, the uncertainty involved in the PVB yield strength is the most likely cause for this discrepancy. If the yield strength is increased to 107 MPa – the value derived by Hopper for a 10 mm fracture pattern at the same strain-rate – Equation A2 predicts a moment capacity of 6.90 Nm, which is higher than the average experimental value, as initially anticipated.

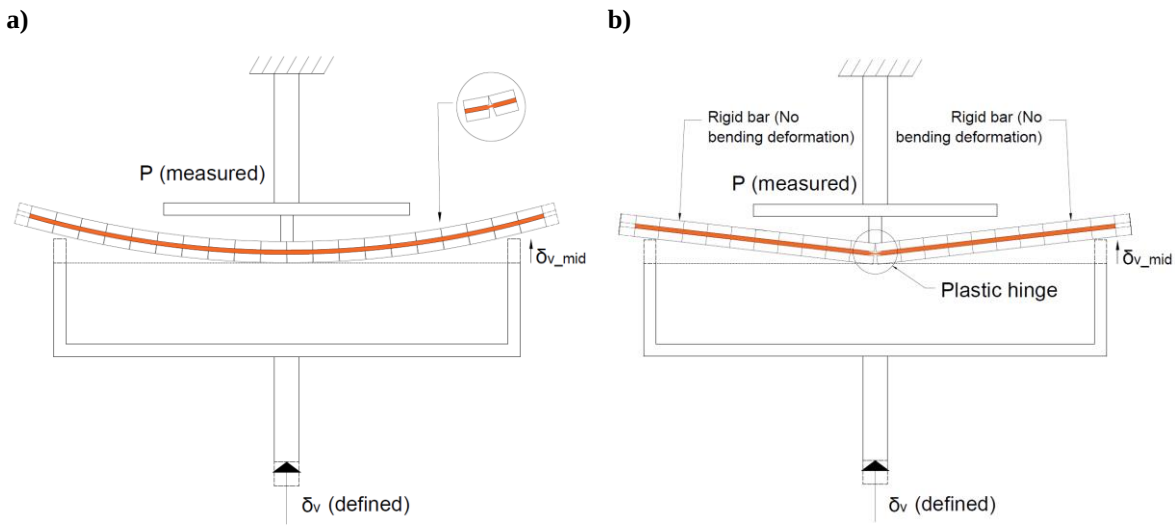

Fig. 9 Deformation of pre-fractured laminated glass, with uniform pattern, during a three-point bend test: (a) elastic response (Stage 3), (b) idealised plastic collapse mechanism (Stage 4). Not to scale.

Stage d follows the formation of the plastic hinge. A brittle failure is observed, with the PVB tearing almost immediately after the hinge is formed. A more ductile response is anticipated under blast loading at room temperature, as this brittle failure is mainly attributed to the low temperature resulting in a stiffer bond between the glass fragments and the PVB, as discussed in Section 3.3.

The same four distinct stages of deformation evident in Figure 8 for the CS1 specimens are also evident in the equivalent results from the thicker CS2 and CS3 specimens. The experimentally derived elastic ($M_{3,E}$) and plastic ($M_{4,E}$) moment capacities are summarised in Table 5, together with the capacities of CS1 for comparison. These are the average values calculated from the three tests repeated for each cross-section. A significant enhancement in the moment capacities is observed for the thicker specimens, providing further evidence of the composite bending response assumed in the models. Increasing the thickness of the PVB and glass layers increases the section modulus ($Z_{PVB,E,3}$) and hence the elastic capacity (M_3); it also results in a larger lever-arm between the resultant tensile force in the PVB and the resultant compressive force in the glass, and therefore a larger plastic moment capacity (M_4).

CS2 and CS3 both have a 1.52 mm thick PVB. At this thickness, the effective yield strength of the PVB is significantly less: Hooper's [5] tensile tests on 20 mm pre-fractured specimens with this thickness indicated a value of 38 MPa at a strain-rate of 30 s^{-1}, rather than 62 MPa for the 0.38 mm thickness of CS1. Using this lower value in Equation A1 results in elastic moment capacities of $M_{3,A} = 8.18$ Nm and 13.09 Nm for CS2 and CS3 respectively, while Equation A2 predicts plastic capacities of $M_{4,A} = 11.45$ Nm and 20.98 Nm. As for CS1, the analytical models under-estimate the capacity of the CS2 and CS3 cross-sections.

In addition to the uncertainty in the PVB yield strength, as described previously, another factor in the observed deviation between the theoretical and experimental results is likely to be the increased strain-rates within the thicker cross-sections for the same loading. The average mapped strain-rates at 25 ˚C for each cross-section are shown in Table 5. Higher yield strength values should therefore be included in the analytical models, as the strain-rates increase from 25 s^{-1} in CS1 to 31 s^{-1} and 56 s^{-1} for CS2 and CS3 specimens, respectively. Hooper [5] reports that at a strain-rate of 100 s^{-1} the PVB peak strength increases from 38 MPa (derived at a strain-rate of 30 s^{-1}) to 95 MPa. The latter value results in increased elastic and plastic capacities of $M_{3,A} = 32.7$ Nm and $M_{4,A} = 50.6$ Nm for the CS3 specimens, which are closer to the experimental results. However, yield strength values were not reported by Hooper [5] for intermediate strain-rates between 30 s^{-1} and 100 s^{-1}. Nevertheless, the experimental results provide strong evidence of an enhanced post-fracture bending capacity at low temperatures that can be estimated conservatively from the analytical models using the PVB yield strength from available high-speed tensile tests. It should be noted, however, that to incorporate these models into analysis methods for the blast design of laminated glass panels, reliable PVB material properties are required. In addition, the post-fracture bending moment capacity of specimens with random fracture patterns requires further investigation.

*Values correspond to a PVB peak strength measured at 100 s^{-1} strain-rate.

	CS1	CS2	CS3
Maximum experimental elastic moment, $M_{3,E}$ [Nm]	4.92	16.35	38.88
Maximum analytical elastic moment, $M_{3,A}$ [Nm]	3.52	8.18	13.09 / 32.7*
Maximum experimental plastic moment, $M_{4,E}$ [Nm]	6.50	20.19	43.09
Maximum analytical plastic moment, $M_{4,A}$ [Nm]	4.10	11.45	20.98 / 50.6*
Experimental strain-rate at -100˚C [s^{-1}]	4.20×10^{-6}	5.13×10^{-6}	9.31×10^{-6}
Mapped strain-rate at 25˚C [s^{-1}]	25.26	30.83	55.94

Table 5 Comparison of experimental and analytical results for CS1, CS2 and CS3 specimens. Analytical values correspond to a PVB peak strength measured at 30 s^{-1} strain-rate.

5 Conclusions

This paper has considered the effect of high strain-rates associated with blast loads on the post-fracture bending response of laminated glass with PVB interlayer. In contrast to traditional dynamic testing, the presented experimental procedure uncouples the strain-rate and inertia effects by performing low strain-rate bending tests at low temperature. The latter simulates high strain-rate effects by taking advantage of the time-temperature dependency of the yield stress of polymers, which has been demonstrated here for PVB using existing tensile test data recorded at various temperatures.

Three-point bending tests were performed on pre-fractured specimens at low and room temperature. It was found that at a temperature of -100 ˚C, the ultimate load capacity of the fractured glass is enhanced by two orders of

magnitude compared to that at room temperature. Given the observed time-temperature dependency of PVB, this is expected to translate to a similar enhancement at the high strain-rates associated with typical blast loading. Such enhanced capacity, if realised in practice, clearly offers potential for more efficient glazing design.

The increased capacity is attributed to the stiffer PVB response at low temperatures (and high strain-rates), resulting in a composite bending action associated with the interlayer working in tension and the glass fragments working in compression. The latter has been demonstrated by comparing the elastic moment capacity derived from the experimental results with existing analytical solutions based on cracked elastic theory. The validity of the theory is further supported by the results from additional specimens with thicker PVB and glass layers, which consistently resulted in enhanced post-fracture capacity due to an increased section modulus. Although the theory under-predicts the experimental results presented here, this is most likely due to uncertainties in the yield strength of PVB, for which there is limited available data. It is therefore concluded that the cracked elastic theory provides an efficient and potentially safe method for estimating the post-fracture bending moment capacity of laminated glass under blast loads.

The experimental results provide valuable insight into the links between the fundamental, material behaviour of laminated glass and its response under full-scale blast loading. The ability of fractured specimens to form plastic hinges at high strain-rates, suggests that yield lines will form in laminated glass panels under blast loading. PVB tearing is anticipated to occur along these yield lines, with bending and membrane strains accumulating at the plastic hinge locations. Including this fractured bending capacity in blast assessments of laminated glass is therefore expected to improve the accuracy of assessments, enabling less conservative design and the optimisation of panel designs. Further research is required to incorporate the effects of a random fracture pattern and inertia loading, which were not considered here.

5 Acknowledgements

The first author gratefully acknowledges the Engineering and Physical Sciences Research Council (EPSRC) for funding this research through the EPSRC Centre for Doctoral Training in Future Infrastructure and Built Environment (FIBE CDT) at the University of Cambridge (EPSRC Grant Reference No. EP/L016095/1). The contribution of the Institution of Civil Engineers, through the ICE Research and Development Enabling Fund, is also gratefully acknowledged, and the authors wish to thank Kuraray and ToughGlaze for donating some of the glass specimens used in the experiments.

Appendix A: Post-fracture bending moment capacity of laminated glass

This appendix reproduces the analytical expressions derived by Angelides et al. [13] for the elastic and plastic post-fracture bending moment capacities of laminated glass. The elastic bending capacity is defined as the bending moment required to cause yielding in the extreme fibre of the interlayer and is derived by considering an equivalent, PVB transformed cross-section:

$$M_{3,A} = \frac{\sigma_{PVB,c,y} I_{PVB,3}}{y_{3,PVB}} = \sigma_{PVB,c,y} Z_{PVB,E,3} \tag{A1}$$

where $y_{3,PVB}$ is the distance of the extreme PVB fibre from the elastic neutral axis, $I_{PVB,3}$ and $Z_{PVB,E,3}$ are the second moment of area and the elastic section modulus of the equivalent, PVB transformed cross-section in Stage 3, and $\sigma_{PVB,c,y}$ is the PVB yield strength accounting for stiffening effects from the attached glass fragments.

The plastic bending capacity is defined as the bending moment required to cause crushing of the glass fragments and is derived by applying moment equilibrium about the plastic neutral axis:

$$M_{4,A} = \frac{2}{3} y_{4,G} C_4 + \left[y_{4,PVB} - \frac{t_{PVB}}{2} \right] T_4 \tag{A2}$$

where $y_{4,G}$ and $y_{4,PVB}$ are the distances of the extreme glass and PVB fibres from the plastic neutral axis, C_4 is the compressive force in the top glass layer that initiates crushing of the glass fragments, and T_4 is the tensile force capacity of the interlayer.

References

[1] C. O'Regan, Structural Use of Glass in Buildings, 2nd ed., Institution of Structural Engineers, London, 2015.

[2] Centre for the Protection of National Infrastructure (CPNI), Introduction to Laminated Glass Interlayers. https://www.cpni.gov.uk/laminated-glass, 2019 (accessed 10 January 2020).

[3] C. Kranzer, G. Gurke, C. Mayrhofer, Testing of bomb resistant glazing systems, in: Proceedings of Glass Processing Days 2005, Tampere, 2005, pp. 497–504.

[4] C. Morison, The resistance of laminated glass to blast pressure loading and the coefficients for single degree of freedom analysis of laminated glass, PhD Dissertation, Cranfield University, 2007. https://dspace.lib.cranfield.ac.uk/handle/1826/4651.

[5] P. Hooper, Blast performance of silicone-bonded laminated glass, PhD Dissertation, Imperial College London, 2011. https://spiral.imperial.ac.uk/handle/10044/1/6861.

[6] P. Del Linz, Blast resistance of laminated glass facades, PhD Dissertation, Imperial College London, 2014. https://spiral.imperial.ac.uk/handle/10044/1/25145.

[7] X. Zhang, H. Hao, Z. Wang, Experimental study of laminated glass window responses under impulsive and blast loading, International Journal of Impact Engineering. 78 (2015) 1–19. https://doi.org/10.1016/j.ijimpeng.2014.11.020.

[8] X. Zhang, H. Hao, Experimental and numerical study of boundary and anchorage effect on laminated glass windows under blast loading, Engineering Structures. 90 (2015) 96–116. https://doi.org/10.1016/j.engstruct.2015.02.022.

[9] M. Larcher, G. Solomos, F. Casadei, N. Gebbeken, Experimental and numerical investigations of laminated glass subjected to blast loading, International Journal of Impact Engineering. 39 (2012) 42–50. https://doi.org/10.1016/j.ijimpeng.2011.09.006.

[10] J. Pelfrene, J. Kuntsche, S. Van Dam, W. Van Paepegem, J. Schneider, Critical assessment of the post-breakage performance of blast loaded laminated glazing: Experiments and simulations, International Journal of Impact Engineering. 88 (2016) 61–71. https://doi.org/10.1016/j.ijimpeng.2015.09.008.

[11] T. Bermbach, M. Teich, N. Gebbeken, Experimental investigation of energy dissipation mechanisms in laminated safety glass for combined blast-temperature loading scenarios, Glass Struct Eng. 1 (2016) 331–350. https://doi.org/10.1007/s40940-016-0029-y.

[12] D. Smith, D. Cormie, Design of glazing, in: D. Cormie, G. Mays, P. Smith (Eds.), Blast Effects on Buildings, 2nd ed., Thomas Telford, London, 2009, pp. 177–215.

[13] S.C. Angelides, J.P. Talbot, M. Overend, The effects of high strain-rate and in-plane restraint on quasi-statically loaded laminated glass: a theoretical study with applications to blast enhancement, Glass Struct Eng. 4 (2019) 403–420. https://doi.org/10.1007/s40940-019-00107-4.

[14] A. Kott, T. Vogel, Remaining Structural Capacity of Broken Laminated Safety Glass, in: Proceedings of Glass Processing Days 2003, Tampere, 2003, pp. 403–407.

[15] S.J. Bennison, J.G. Sloan, D.F. Kristunas, P.J. Buehler, T. Amos, C.A. Smith, Laminated Glass for Blast Mitigation: Role of Interlayer Properties, in: Proceedings of Glass Processing Days 2005, Tampere, 2005.

[16] R. Iwasaki, C. Sato, J.L. Latailladeand, P. Viot, Experimental study on the interface fracture toughness of PVB (polyvinyl butyral)/glass at high strain rates, International Journal of Crashworthiness. 12 (2007) 293–298. https://doi.org/10.1080/13588260701442249.

[17] P.A. Hooper, B.R.K. Blackman, J.P. Dear, The mechanical behaviour of poly(vinyl butyral) at different strain magnitudes and strain rates, Journal of Materials Science. 47 (2012) 3564–3576. https://doi.org/10.1007/s10853-011-6202-4.

[18] J. Kuntsche, J. Schneider, Mechanical behaviour of polymer interlayers in explosion resistant glazing, in: Challenging Glass 4 and COST Action TU0905 Final Conference, Lausanne, 2014, pp. 447–454.

[19] X. Zhang, H. Hao, Y. Shi, J. Cui, The mechanical properties of Polyvinyl Butyral (PVB) at high strain rates, Construction and Building Materials. 93 (2015) 404–415. https://doi.org/10.1016/j.conbuildmat.2015.04.057.

[20] S. Chen, X. Chen, X. Wu, The mechanical behaviour of polyvinyl butyral at intermediate strain rates and different temperatures, Construction and Building Materials. 182 (2018) 66–79. https://doi.org/10.1016/j.conbuildmat.2018.06.080.

[21] M. Botz, M.A. Kraus, G. Siebert, Untersuchungen zur thermomechanischen Modellierung der Resttragfähigkeit von Verbundglas, ce/papers. 3 (2019) 125–136. https://doi.org/10.1002/cepa.1005.

[22] M.A. Samieian, D. Cormie, D. Smith, W. Wholey, B.R.K. Blackman, J.P. Dear, P.A. Hooper, Temperature effects on laminated glass at high rate, International Journal of Impact Engineering. 111 (2018) 177–186. https://doi.org/10.1016/j.ijimpeng.2017.09.001.

[23] A. Kott, T. Vogel, Safety of laminated glass structures after initial failure, Structural Engineering International. 2 (2004) 134–138.

[24] A. Kott, T. Vogel, Structural Behaviour of Broken Laminated Safety Glass, in: Crisinel, M., Eekhout,M., Haldimann, M., Visser, R. (Eds.), Glass and Interactive Building Envelopes, IOS Press, Delft, 2007.

[25] M. Botz, Beitrag zur versuchstechnischen und numerischen Beschreibung von Verbundglas mit PVB-Zwischenschicht im intakten und gebrochenen Zustand, PhD Dissertation, Universität der Bundewehr München, 2020. https://athene-forschung.unibw.de/85231?show_id=134116.

[26] C. Carrot, A. Bendaoud, C. Pillon, Polyvinyl Butyral, in: O. Olabisi, K. Adewale (Eds.), Handbook of Thermoplastics, 2nd ed., CRC Press, London, 2015. https://doi.org/10.1201/b19190.

[27] J.D. Menczel, R.B. Prime, eds., Thermal analysis of polymers: fundamentals and applications, John Wiley, Hoboken, 2009.

[28] B. Liu, J. Xu, Y. Li, Constitutive Investigation on Viscoelasticity of PolyVinyl Butyral: Experiments Based on Dynamic Mechanical Analysis Method, Advances in Materials Science and Engineering. 2014 (2014) 1–10. https://doi.org/10.1155/2014/794568.

[29] J. Kuntsche, Mechanisches Verhalten von Verbundglas unter zeitabhängiger Belastung und Explosionsbeanspruchung (Mechanical behaviour of laminated glass under time- dependent and explosion loading), PhD Dissertation, Technische Universität Darmstadt, 2015.

[30] F. Pelayo, M.J. Lamela-Rey, M. Muniz-Calvente, M. López-Aenlle, A. Álvarez-Vázquez, A. Fernández-Canteli, Study of the time-temperature-dependent behaviour of PVB: Application to laminated glass elements, Thin-Walled Structures. 119 (2017) 324–331. https://doi.org/10.1016/j.tws.2017.06.030.

[31] M.A. Kraus, Machine Learning Techniques for the Material Parameter Identification of Laminated Glass in the Intact and Post-Fracture State, PhD Dissertation, Universität der Bundewehr München, 2019. https://athene-forschung.unibw.de/127852.

[32] S.M. Walley, J.E. Field, P.H. Pope, N.A. Safford, A study of the rapid deformation behaviour of a range of polymers, Phil. Trans. R. Soc. Lond. A. 328 (1989) 1–33. https://doi.org/10.1098/rsta.1989.0020.

[33] M.J. Kendall, C.R. Siviour, Experimentally simulating high-rate behaviour: rate and temperature effects in polycarbonate and PMMA, Phil. Trans. R. Soc. A. 372 (2014) 20130202. https://doi.org/10.1098/rsta.2013.0202.

[34] M.L. Williams, R.F. Landel, J.D. Ferry, The Temperature Dependence of Relaxation Mechanisms in Amorphous Polymers and Other Glass-forming Liquids, J. Am. Chem. Soc. 77 (1955) 3701–3707. https://doi.org/10.1021/ja01619a008.

[35] C.R. Siviour, S.M. Walley, W.G. Proud, J.E. Field, The high strain rate compressive behaviour of polycarbonate and polyvinylidene difluoride, Polymer. 46 (2005) 12546–12555. https://doi.org/10.1016/j.polymer.2005.10.109.

[36] E.N. Brown, R.B. Willms, G.T. Gray, P.J. Rae, C.M. Cady, K.S. Vecchio, J. Flowers, M.Y. Martinez, Influence of Molecular Conformation on the Constitutive Response of Polyethylene: A Comparison of HDPE, UHMWPE, and PEX, Exp Mech. 47 (2007) 381–393. https://doi.org/10.1007/s11340-007-9045-9.

[37] J.L. Jordan, C.R. Siviour, J.R. Foley, E.N. Brown, Compressive properties of extruded polytetrafluoroethylene, Polymer. 48 (2007) 4184–4195. https://doi.org/10.1016/j.polymer.2007.05.038.

[38] D.M. Williamson, C.R. Siviour, W.G. Proud, S.J.P. Palmer, R. Govier, K. Ellis, P. Blackwell, C. Leppard, Temperature–time response of a polymer bonded explosive in compression (EDC37), J. Phys. D: Appl. Phys. 41 (2008) 085404. https://doi.org/10.1088/0022-3727/41/8/085404.

[39] M.J. Kendall, C.R. Siviour, Experimentally simulating adiabatic conditions: Approximating high rate polymer behavior using low rate experiments with temperature profiles, Polymer. 54 (2013) 5058–5063. https://doi.org/10.1016/j.polymer.2013.06.049.

[40] BS EN ISO 12543-2:2011: Glass in building - Laminated glass and laminated safety glass - Part 2: Laminated safety glass, British Standards Institution, London, 2011.

[41] S. Nhamoinesu, M. Overend, Simple Models for Predicting the Post-fracture Behaviour of Laminated Glass, in: Proceedings of the XXV A.T.I.V 2010 International Conference, Parma, 2010.

[42] M. Botz, K. Wilhelm, G. Siebert, Experimental investigations on the creep behaviour of PVB under different temperatures and humidity conditions, Glass Struct Eng. 4 (2019) 389–402. https://doi.org/10.1007/s40940-019-00098-2.